RSC Advances

PAPER

View Article Online
View Journal | View Issue

Cite this: *RSC Adv.*, 2020, **10**, 7360

An NIF-doped ZIF-8 hybrid membrane for continuous antimicrobial treatment†

Dan Luo,[a] Cuijuan Wang,*[a] Yan Tong,*[a] Cheng Liu,[a] Yumei Xiao,[a] Zixin Zhu,[a] DongNing Liu[a] and Yaoyu Wang[b]

Received 5th January 2020
Accepted 3rd February 2020

DOI: 10.1039/d0ra00108b

rsc.li/rsc-advances

Sodium alginate (ALG) composites with ZIF-8 and niflumic acid (NIF) were prepared by a one-pot method at room temperature and characterized by FTIR, SEM and XRD studies. In the composite, ZIF-8 was used as a highly connected node in a supercrosslinked polymer network. In addition, the material exhibits good antibacterial activity against *Staphylococcus aureus* and *Escherichia coli in vitro*. Compared to the original ALG membrane and ZIF-8, the ZIF–NIF–ALG membrane has the following advantages: stronger antibacterial properties; slow release of Zn(II); high drug loading; and longer sustained release time. This research introduces new concepts for the design and manufacture of various antimicrobial membranes and broadens the range of applications of MOFs.

Introduction

Postoperative wound infection is a medical problem. During the wound healing process, the continuous inflammatory process hinders the healing process;[1] in addition to the eradication of bacteria, prevention of inflammatory processes and control of the inflammatory response are particularly important. Antibiotic abuse creates many problems and requires the development of new antibacterial agents; currently, nanotechnology has its own unique charm in the field of antibacterial agents.[2,3] In this regard, porous metal–organic frameworks are an attractive nanomaterial because they are promising in catalysis, sensing,[4] adsorption[5,6] and imaging; they have also found a place in the antibacterial field.[7–9] In previous studies, MOFs could act as metal ion reservoirs to provide progressive release of metal ions for sterilization.[10] Among various MOF structures, ZIF-8 exhibits unique advantages,[11] such as excellent chemical stability, large surface area, pH responsiveness and simple synthetic methods;[12] due to all these properties, ZIF-8 stands out in the antibacterial field.[13] There have been reports of research to develop an effective anti-inflammatory and antibacterial platform for the treatment of periodontitis by incorporating cerium (Ce) into the zeolite imidazole ester backbone 8 (ZIF-8).[14] Tet@ZIF-8@HA nanocomposites (TZH) were synthesized as a nanocarrier platform for selective/controlled release[33] of antibiotics in specific regions. According to a literature search,[15,16] although many research groups have investigated ZIF-8 nanocomposites, the instability of MOFs in water and the inherent properties of powder materials may limit their practical application.[17] Due to the inherent powder properties of MOFs, it is difficult for them to fully contact the surface of infected skin to kill bacteria; therefore, the use of MOFs alone is very inefficient. Studies have shown that complexes that are uniformly dispersed exhibit a higher level of biological activity, enhance the lipophilicity of the complex, and promote their penetration into the bacterial cell wall.

To avoid these problems, an effective method is to immobilize MOFs on a solid substrate such as polyacrylamide, hydrogel, fiber, chitosan (CS) or cotton,[18–20] these hybrid membranes can enhance the adsorption of antibiotics and show enhanced antibacterial properties[21–23]. MOFs are being considered for use in antibacterial dressings because the excipients prevent bacterial colonization and subsequent biofilm formation and overcome the inherent defects of the powder at the same time. In addition, nanomaterials lack the ability to treat inflammatory reactions in wound infections, studies have shown that nanomaterials may produce ROS,[24] aggravate the inflammatory response of the wound, and delay the treatment of the disease. Therefore, there is an urgent need to develop a novel nanomaterial that has both antibacterial and anti-inflammatory functions and overcomes the agglomeration of solid powder.

In a previous study, it was found that NIF and 2-methylimidazole (2-MI) can react with Zn(II) to synthesize rod crystals, thereby changing the original form of ZIF-8. NIF is an anti-inflammatory therapeutic component[25] with a reactive carboxyl group that can undergo a coordinating reaction with Zn(II).[26] Therefore, we added NIF and 2-MI to the ALG material as a ligand for Zn(II). NIF does not only acts as an anti-inflammatory factor. Data show that due to its presence, ZIF–

[a]*School of Life Science and Engineering, Southwest Jiaotong University, Chengdu, 610000, China. E-mail: wangcuijuan@home.swjtu.edu.cn*

[b]*Key Laboratory of Synthetic and Natural Functional Molecule Chemistry of Ministry of Education, Department of Chemistry, Northwest University, Xi'an 710069, China*

† Electronic supplementary information (ESI) available. See DOI: 10.1039/d0ra00108b

NIF has a stronger antibacterial effect than ZIF-8. At this time, in the slightly acidic environment after infection (pH 5.5),[27] based on the characteristics of ZIF-8, the coordination of 2-MI and Zn(II) is weakened, and the Zn(II) is slowly released to become an antibactericidal factor. The crystal structure disintegrates, and NIF is slowly released as an anti-inflammatory factor. ALG absorbs tissue exudate and promotes wound healing.[28] In this regard, ALG can be used not only as a container for crystals, but also as a container for other molecules that can release molecules (such as antibiotics) for effective bacteriostasis.

In this study, cross-linked polymer materials of ALG, NIF and ZIF-8 were synthesized for the first time and used for local wound infection treatment with antibacterial and anti-inflammatory effects. As shown in Fig. 1, the purposes of this study were: (1) to develop and characterize composite hydrogels for the prevention and treatment of wound infections; (2) to investigate the antibacterial properties and biocompatibility of the hydrogels *in vitro*. The results demonstrate that this material is an antibacterial anti-inflammatory biological dressing which has good antibacterial effects and biocompatibility.

Experimental

Synthetic procedure of ZIF-8, ZIF–NIF and ZIF–NIF–ALG

The synthetic method was adapted from previous literature reports.[29] A reaction mixture containing $Zn(NO_3)_2 \cdot 6H_2O$ (0.2680 g, 0.9 mmol) and H_2O (10 mL, pH 7.4) was placed in a 50 mL beaker. A mixture of 2-MI (2.00 g, 0.0245 mol) in methanol (10 mL) was added dropwise to the solution with stirring at room temperature over 24 h. The product was centrifuged at 6000 rpm for 5 minutes and washed 3 times with 10 mL of EtOH/H_2O solution (1 : 1). A mixture of NIF (0.2820 g, 0.1 mmol) and 2-MI (0.0821 g, 0.1 mmol) was added to 10 mL of a methanol solution, which was stirred and dissolved; then, $Zn(NO_3)_2 \cdot 6H_2O$ (0.2680 g, 0.9 mmol) was added, and the mixture was stirred at room temperature. After 12 h, the product was washed several times with methanol and dried at room temperature to obtain a pale yellow powder (ZIF–NIF). 1.5 g of ALG (1.5000 g, 6.94 mol) was dissolved in 50 mL of sterile water and stirred for 2 h; ZIF-NIF (0.005 g) was added, followed by stirring for 24 h. 2 mL of solution was taken and dried naturally in the template to prepare a 1 mm thick film.

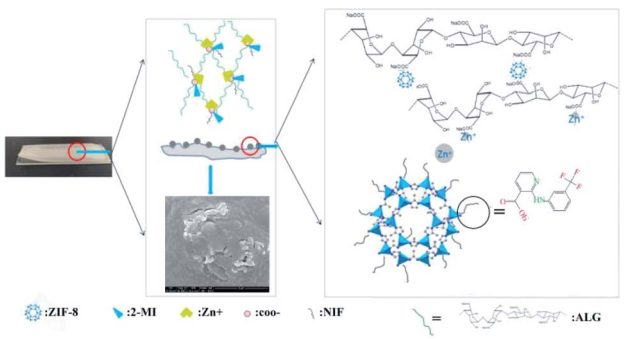

Fig. 1 One-pot synthesis of the ZIF–NIF–ALG biofilm, in which Zn(II) reacts with ALG, 2-MI, and NIF to form rod-like structures resembling ZIF–NIF on the surface of the membrane.

Scanning electron microscopy (SEM)

Scanning electron microscopy (SEM) was performed using a field emission scanning electron microscope (FESEM, JEOL JSM-7400F, Japan) to study the surfaces of ALG, Zn–ALG, ZIF-8, ZIF–NIF, ZIF-8–ALG, and ZIF–NIF–ALG. The morphology was studied, and a 2 to 3 nm platinum layer was sprayed onto the sample to provide a conductive surface. Morphological changes of bacteria after treatment with ZIF–NA–ALG were also examined. Briefly, bacteria suspended in phosphate buffered saline (PBS) (106 CFU mL^{-1}, 200 μL) were inoculated onto ZIF–NA–ALG. After incubating for 24 h at 37 °C, the samples were washed twice with PBS and then fixed with 2.5% glutaraldehyde in PBS for 2 h at room temperature. The fixed bacteria were dehydrated for 15 minutes with a series of graded ethanol solutions (25%, 50%, 75%, 95% and 100%). After drying for 12 h, the samples were plated with platinum for imaging.

Preparation of tetracycline encapsulated by ZIF–NIF–ALG, ZIF-8 and ALG

To load tetracycline onto ZIF–NIF–ALG, a ZIF–NIF–ALG membrane (0.1 g) was mixed with a tetracycline solution (10 mL, 20 mg mL^{-1}). The tetracycline-ZIF–NIF–ALG suspension was sealed and stirred at room temperature for 5 days. Next, tetracycline loaded on ZIF–NIF–ALG was filtered using a centrifugal filter and washed 3 times with methanol to eliminate unabsorbed drug on ZIF–NIF–ALG. Finally, the pale yellow ZIF–NIF–ALG film was dried overnight in an oven at 35 °C. Based on eqn (1), the drug loading was 27.8%:

$$\text{Drug loading (\%)} = (\text{weight of tetracycline in sample/total weight of sample}) \times 100\% \quad (1)$$

The drug loading method of ZIF-8 and ALG is as described above.

Release experiment

The process of the release of tetracycline from ZIF–NIF–ALG/tetracycline, ZIF-8/tetracycline and ALG/tetracycline was evaluated in PBS (pH 7.4) and PBS (pH 5.5) solutions. For this purpose, suspensions of ZIF–NIF–ALG/tetracycline (0.02 g), ZIF-8/tetracycline (0.02 g) and ALG/tetracycline (0.02 g) were prepared in PBS (50 mL, pH 7.4) and PBS (50 mL, pH 5.5) solutions at 37 °C and then mixed using a magnetic stirrer (200 rpm) for three days. In order to avoid interference with NIF, the unloading materials of ZIF–NIF and ZIF–NIF–ALG were placed in PBS solution under the same conditions, and the supernatant was used as a test group. In addition, the concentration of released drug was determined by collecting and analyzing samples from the supernatant at various time points over the course of three days. The amounts of tetracycline released from ZIF–NIF–ALG/tetracycline, ZIF-8/tetracycline and ALG/tetracycline at each time point were determined using a UV/

vis spectrometer with light at a wavelength of 350 nm. Finally, the release percentage was expressed using eqn (2):

$$\text{Release percentage (\%)} = (\text{weight of tetracycline release/total weight of tetracycline}) \times 100\% \quad (2)$$

The formula for testing the release of nicotinic acid was the same as above, and the test wavelength was converted to 350 nm. For this purpose, suspensions of ZIF–NIF–ALG (0.02 g) were prepared in PBS (50 mL, pH 7.4) and PBS (50 mL, pH 5.5) solutions at 37 °C and then mixed using a magnetic stirrer (200 rpm) for three days. In addition, the concentration of released drug was determined by collecting and analyzing samples from the supernatant at various time points over the course of these three days. The method for testing the release of cell contents is the same as above, and the test wavelength was converted to 260 nm.

Antibacterial experiments with different materials

In this study, *E. coli* (ATCC 6538) was selected as a Gram-negative bacterium, and *S. aureus* (ATCC 25922) was used as a model for Gram-positive bacteria. *E. coli* colonies were scraped off and inoculated overnight in 3 mL LB broth. One hundred microliters of the overnight culture was suspended in 3 Ml of Mueller–Hinton Broth (MHB) and incubated for 2 to 3 h to obtain a bacterial culture at a concentration of 5×10^6 CFU mL^{-1}. The cultured *Escherichia coli* was diluted to 50 mL, and ZIF-8, ZIF–NIF, ZIF–NIF–ALG, 2-MI, and NIF were added thereto. After 24 h of treatment, the sample was removed by centrifugation at 2000 rpm. An aliquot (0.5 mL) was collected, and the absorbance was measured at 600 nm with UV-visible light. In the blank control experiment, the cultured *Escherichia coli* was diluted to 50 mL and cultured under the same conditions. After 24 h, an aliquot (0.5 mL) was obtained, and the absorbance was measured at 600 nm using an ultraviolet spectrophotometer.[30]

Cytotoxicity assay

The MTT assay[31] was performed to examine the viability of human cells after administration of ZIF–NIF–ALG, ZIF-8 and ALG. Cytotoxicity assays were performed using phagocytic cells (1.0×103 cells per mL) according to standard protocols. Cells were seeded into 24-well plates at a density of 2×105 cells per well and incubated for 24 h. Then, the medium was supplemented, and ZIF-8, ZIF–NIF, and ZIF–NIF–ALG were added to each well in concentrations ranging from 0 μg mL^{-1} to 500 μg mL^{-1}. After 12 h of incubation, the culture broth was removed from each well, and the cells were washed with PBS. Then, 50 μL MTT (5 mg mL^{-1}) was added to each well, followed by incubation at 37 °C for 4 h. Next, the crystals were further dissolved using 1 mL of dimethyl sulfoxide (DMSO), and the absorbance at 492 nm was measured by a microplate reader. Cell viability was determined as a percentage of the absorbance relative to the control.

Hemolysis assay

The hemolytic activity of ZIF–NIF–ALG was measured. Fresh mouse erythrocytes (RBC) were diluted with sterile water to obtain a stock suspension of RBC (4 vol% blood cells). For ZIF–NIF–ALG, 100 μL aliquots of RBC suspension were mixed with 100 μL of ZIF–NIF–ALG suspension (4 mg to 8 mg). After incubating for 1 hour at 37 °C, the mixture was centrifuged at 2000 rpm for 5 minutes. An aliquot of the supernatant (100 μL) was transferred to a 96-well plate. The OD readings were recorded at 576 nm using a microplate reader to assess hemoglobin release. A control solution containing only DPBS was used as a reference for 0% hemolysis. The absorbance of red blood cells lysed with 0.5% Triton-X was considered to be 100% hemolysis. Data are expressed as quadruplicate mean and standard deviation (SD), and the tests were repeated twice independently.

Statistical analysis

All the quantitative data in each experiment were evaluated and analysed by one-way analysis of variance and expressed as the mean values ± standard deviations. Student's *t*-test was used to evaluate the statistical significance of the variance. Values of $^*P < 0.05$, $^{**}P < 0.01$ and $^{***}P < 0.001$ were considered statistically significant.

Results and discussion

According to the synthesis procedure shown in Fig. 1, ZIF–NIF–ALG was synthesized in one pot at room temperature using zinc nitrate, 2-MI, NIF and ALG. Initially, 2-MI and NIF reacted rapidly with Zn(II) to form crystal particles. The ZIF–NIF particles provide Zn(II) as a cross-linking point of two sodium alginate molecules, thereby connecting into a gel-like polymer network structure. At the same time, free Zn(II) also function as cross-linking agents between sodium alginate, increasing the stability of the structure. Powder X-ray diffraction (PXRD) analysis confirmed the purity of the synthesized ZIF-8. The biofilm of ZIF–NIF has a characteristic peak of ZIF-8 and a characteristic peak of NIF. However, after storage for 12 h in an acidic environment (pH 5.5), the crystal structure no longer exists. The simple alginate hydrogel film does not have a crystal structure, the biofilm introduced into the crystal has a characteristic peak of ZIF–NIF, and the peak value is lower than that of the pure ZIF–NIF powder because the crystal doping amount is small. It can be concluded that ZIF–NIF was successfully introduced into the ALG hydrogel (Fig. 3A). When 2-MI and NIF simultaneously act as ligands to react with Zn(II), the crystal morphology of the synthesis changes significantly, from a regular hexagonal structure (ZIF-8) to a rod-like structure with a length of about 50 microns (Fig. 2E–G). We suspect that the addition of NIF resulted in a change in the coordination environment; therefore, morphological changes occurred. Different proportions of NIF were added during the synthesis, and the crystal shapes were also different (Fig. 2F and G). In the nitrogen adsorption desorption curve (Fig. 3C and D), it can be seen that the specific surface area of ZIF–NIF after doping with NIF is decreased, the pore diameter is increased from 4.1409 nm to 4.6132 nm, the specific surface area is lowered, and the crystal pores are reduced (Table S1†). This shows that NIF is not simply

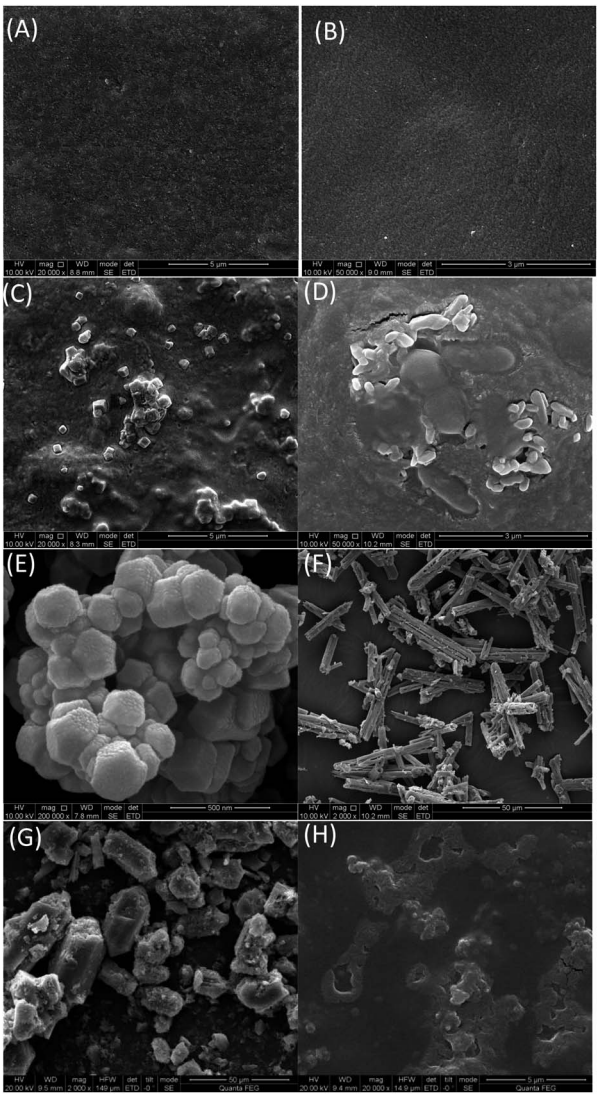

Fig. 2 Scanning electron microscope (SEM) images of (A) ALG; (B) Zn–ALG; (C) ZIF-8–ALG; (D) ZIF–NIF–ALG; (E) ZIF-8; (F) ZIF–NIF doped with 10% NIF; (G) ZIF–NIF doped with 20% NIF; (H) ZIF–NIF–ALG film after 24 h of treatment in a slightly acidic environment.

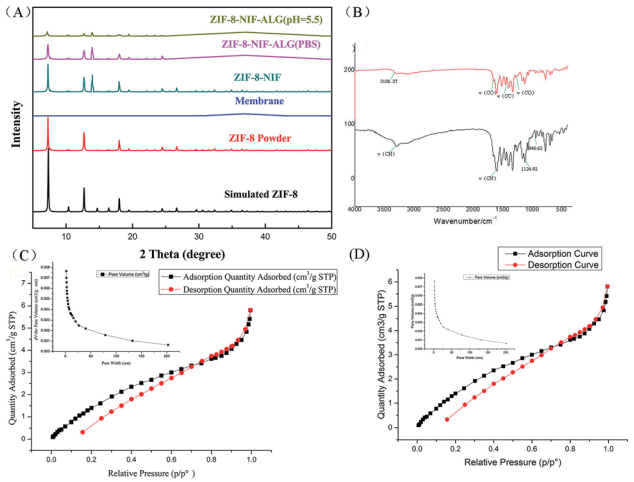

Fig. 3 (A) X-ray diffraction (XRD) patterns and (B) Fourier transform infrared (FT-IR) spectra of ZIF–NIF–ALG/ZIF-8; (C) nitrogen adsorption and desorption of ZIF-8; (D) nitrogen adsorption and desorption of ZIF–NIF.

adsorbed on the ZIF-8 surface or in the pores, but participates in the coordination process and changes the pore size.[32] In terms of drug-loading properties, tetracycline has a higher molecular weight and tends to enter larger pores. ZIF–NIF contains the carboxylic acid groups of NIF, and these groups react with tetracycline to produce a certain amount of adsorption;[33] these two reasons lead to higher drug loading of ZIF–NIF and ZIF–NIF–ALG.

To further demonstrate the presence of NIF in the substrate, we also characterized ZIF–NIF with FTIR spectroscopy. In the FTIR spectrum (Fig. 3B), ZIF–NIF shows characteristic peaks of ZIF-8 at 694.45 cm^{-1} and 772.41 cm^{-1}. The adsorption bands are the deformation vibration adsorption of CH and NH groups in ZIF-8, and the band of Zn–N is at 418.04 cm^{-1}. For the ZIF-8 powder, there are four characteristic peaks;[34] the peaks at 3106.27 cm^{-1} and 1597.2 cm^{-1} are related to the ν(CH) and ν(CN) tensile vibrations of imidazole (IMI), respectively. The peak ranging from 1350 cm^{-1} to 1500 cm^{-1} is related to the extension of the entire imidazole ring, and the peaks at 1124.92 cm^{-1} and 940.62 cm^{-1} are attributed to the in-plane bending of the imidazole ring. Compared with ZIF-8, the spectrum of ZIF–NIF has a ν(C=O) stretching vibration at 1662 cm^{-1} and a stretching vibration of ν(CO) at 1255 cm^{-1}. The peak at 1124.92 cm^{-1} is assigned to the ν(CCF) vibration. These are the characteristic peaks of NIF. The characteristic peak of coordination between carboxyl and zinc exists at 3106.27 cm^{-1}, the stretching vibration of aromatic rings is found at 1560.68 cm^{-1} and the stretching vibration of ν(CC) bonds on aromatic rings is at 1450.91 cm^{-1}. These data indicate coordination between NIF and Zn(II).[35] In order to use a material for long-term release of a drug, it is necessary to test the stability of the material in an organism. In the material stability test, it can be seen by SEM that the surface of the material partially collapses after being incubated in mouse blood for 3 days. The ALG matrix does not change much (Fig. 2H). The thermal stability of the material was investigated by TGA. As shown in Fig. S1,† for ZIF-8, the mass loss at 100 °C to 200 °C is related to the evaporation of water molecules. At 367.5 °C, the third step of weight loss was achieved due to carbonization of the ZIF-8 organic ligand.[36] In the TGA curve of ZIF–NIF (Fig. S2†), considering the weight loss of NIF in ZIF–NIF, it exhibits a mass loss at 100 °C to 200 °C compared to the TGA curve of ZIF-8. The loss is much higher than the weight lost by ZIF-8 at this point. This step corresponds to the loss of a portion of niflumic acid and water molecules. There is a loss of weight around 540 °C, which corresponds to complete decarboxylation of niflumic acid. The weight loss process above 600 °C corresponds to the collapse of the material skeleton, and the remaining white solid residue (6.7%) corresponds to ZnO (0.1023 mg). Compared to the TGA curve of ZIF-8, the curve of ZIF–NIF is different due to the presence of NIF. There are two other decarboxylation steps.

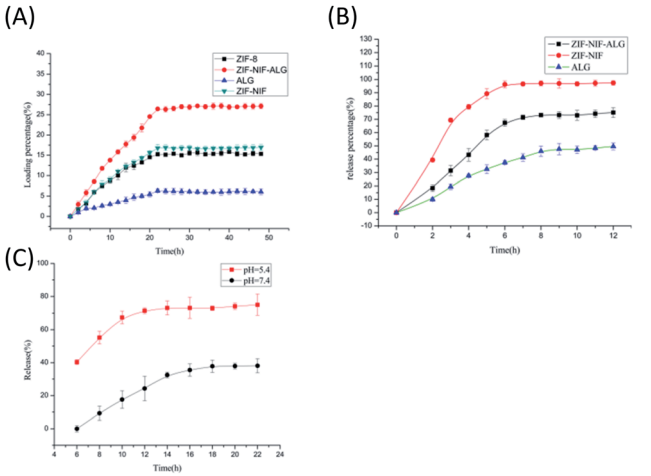

Fig. 4 (A) Drug loading curves of ZIF-8/ZIF–NIF/ZIF–NIF–ALG/ALG in PBS; (B) drug release curves of ALG/ZIF–NIF/ZIF–NIF–ALG at pH 5.5; (C) drug release curves of ZIF–NIF–ALG at pH 5.5 and pH 7.4, respectively.

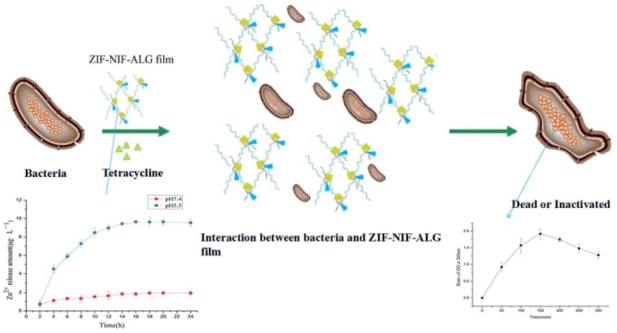

Fig. 5 The tetracycline-loaded ZIF–NIF–ALG membrane envelops the bacteria, releasing Zn(II) in a slightly acidic environment, causing the bacterial contents to overflow and resulting in bacterial death.

Tetracycline was used as a template drug to evaluate the drug-loading properties and drug release properties of the composite hydrogels. Tetracycline demonstrated high antibacterial properties in previous studies.[37] Compared to ZIF-8 and hydrogels, the composite hydrogels have significantly greater drug loading; as shown in Fig. 4A, compared to the pure hydrogels, crystal ZIF–NIF on the composite hydrogel surfaces has a larger pore size than ZIF-8. This results in gaps on the surface of the hydrogel, which is beneficial for drug adsorption. According to the literature, in a slightly acidic environment, the coordination bond of 2-MI and Zn(II) is broken,[38] which causes collapse of the crystal structure. As shown in Fig. 3B, the release rate of tetracycline in the composite hydrogel was accelerated in the environment of phosphate buffer solution (pH 5.5). This material has a certain pH responsiveness. Compared with ZIF-8, the composite hydrogel has a longer release time, which improves the release properties of the material; thus, it is more suitable as a long-term release carrier *in vitro* (Table 1).

After evaluating the drug-loading properties of the material, the antibacterial effects of ZIF-8/ZIF–NIF/ZIF–NIF–ALG were further evaluated (Fig. S8†). The antibacterial effects of these three materials on *Escherichia coli* were observed within 24 h. ZIF–NIF showed a certain antibacterial effect; however, its inhibition rate is lower than that of ZIF–NIF–ALG, because it is difficult for the ZIF–NIF powder to contact the bacteria. The simple ALG hydrogel does not have antibacterial activity because its surface is not suitable for bacterial reproduction; therefore, it shows a certain antibacterial rate, but the antibacterial effect is poorer than those of ZIF–NIF and ZIF–NIF–ALG. Through the above-mentioned *in vitro* antibacterial activity screening, further studies on ZIF–NIF–ALG materials with high antibacterial activity were continued, and ZIF–NIF–ALG was evaluated for two common wound pathogens, Gram-negative *Escherichia coli* and Gram-positive *Staphylococcus aureus*. The antibacterial activity of the cocci showed that the hydrogel had extraordinary bactericidal activity against *Escherichia coli* and *Staphylococcus aureus*. In the 24 hour incubation test, ZIF–NIF–ALG had a bacterial inhibition rate of 95.4% against *S. aureus*, while the inhibition rate against *E. coli* was 91.1% (Fig. 5A–F). The detection of the antibacterial effect of the synthetic component was carried out by converting the measured absorbance into an antibacterial rate by the following formula: inhibition rate = {(OD value of the blank group − OD value in the sample)/OD value of the blank group} × 100%. The calculated bacteriostatic rate of each material was as follows: 98%, 59.4%, 52.8%, 53.4%, 59.2%, and 89.4%, corresponding to zinc nitrate, ZIF-8, ZIF–NIF, ZIF–NIF–ALG, 2-MI, and NIF (Fig S4†). Imidazole derivatives have shown good antibacterial activity in previous reports, and they play an important role in bacterial nucleic acid and protein synthesis. 2-MI itself has antibacterial activity. It can be seen that the composite hydrogel has the antibacterial properties of ZIF-8 and NIF, therefore, it has a high antibacterial rate. The bacterial survival rate was 52.8%. Antibacterial experiments were performed on composite films doped with different levels of NIF. A slight increase in its antibacterial activity was found with increasing nicotinic acid content. When exhibiting the best antibacterial activity, its

Table 1 Comparison of the antibacterial properties and slow-release properties of various antibacterial metal compounds

	7 nm silver nanoparticles[49]	29 nm silver nanoparticles	Ceftazidime@ ZIF-8(ref. 50)	HKUST-1 (ref. 47)	MOF199 (ref. 51)	BioMIL-5 (ref. 48)	ZIF–NIF–ALG
MIC (μg mL^{-1})	6.25	13.02	50	100	25	1.7	50
Sustained release time	—	—	7 d	10 h (ref. 46)	—	60 d	3 d

mass fraction was 20% (Fig. S10†). The release of NIF will correspondingly reduce inflammation after wound infection, and the addition of this factor improves the antibacterial performance of ZIF-8, because NIF inhibits the Na^+/dicarboxylate symporter of bacteria. This transporter plays an important role in the tricarboxylic acid cycle. If the protein is inhibited, it will affect bacterial respiration and thus inhibit bacterial reproduction.[39]

According to the literature reviewed, the speculated antibacterial mechanism is that the biological dressing covers the wound and the ZIF–NIF crystal particles on the surface gradually disintegrate in the weak acid environment of bacterial infection, releasing Zn(II), NIF and tetracycline. Faced with these antibacterial and anti-inflammatory factors, bacteria began to show cell damage, which inhibits their proliferation (Fig. 5). To confirm this speculation, the following experiments were performed. Morphological differences in *E. coli* before and after treatment with the composite material were examined by SEM (Fig. 6G and H). The *E. coli* that was not treated with the composite hydrogel had intact cell walls and basic morphology. After treatment with the composite hydrogel for 24 h, the morphology of *E. coli* was destroyed and the basic morphology could not be maintained. For the materials ZIF-8, ZIF–NIF, and ZIF–NIF–ALG, when the cell membrane is damaged, K^+ and PO_4^{-3} will leak first, followed by DNA and RNA; these components of cells can be easily detected with 260 nm UV light. This test characterizes the damage of the cell membrane and also corresponds to the antibacterial ability of the material. Therefore, we measured the intracellular dissolved content. It can be visually seen that the amount of internal dissolved matter increased after treatment with ZIF–NIF–ALG for 24 h (Fig. 6I), combined with the SEM data. It was found that the material destroyed the bacterial cell membrane integrity and caused bacterial death. Considering the possible damage to cells caused by the sustained release of Zn(II), we examined the release of Zn(II) from the composite hydrogel in the presence of phosphate buffer (pH 5.5) (Fig. S5†),[40] and the release of Zn(II) reached 10 μg mL^{-1}. Corresponding to the antibacterial effects of zinc nitrate in the above bacteriostatic test, it is proved that there may be a phenomenon where the slow release of Zn(II) achieves the bacteriostatic purpose; also, the released Zn(II) can rapidly penetrate the bacteria, resulting in disorder of the intracellular metabolic pathway of the bacteria[41] and thereby improving the sterilization efficiency. Encouraged by the above experiments, we continued to study the effects of different doses on the antibacterial effects. As the dose increased, the survival rate of the bacteria also decreased, and there was a dose-dependent bacteriostatic phenomenon (Fig. 6A–F). The material kills bacteria by slowly releasing metal ions. In addition, we studied the anti-inflammatory effects of the materials. According to the literature, nanomaterials exacerbate wound inflammation because nanomaterials produce ROS, which exacerbate inflammation.[42,43] Therefore, it is necessary to detect the release of the anti-inflammatory factor, the release of NIF under acidic conditions was examined at 350 nm. It was found that with time, the release amount gradually increased and stabilized, and its release tendency was similar to that of Zn(II) (Fig. S6†),

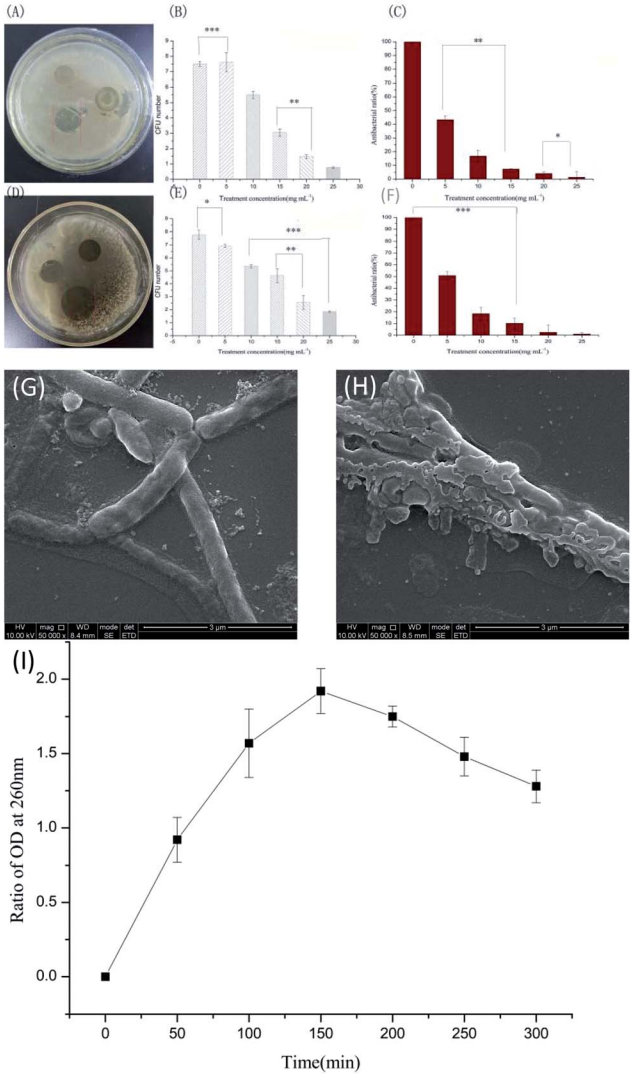

Fig. 6 After treatment with ZIF–NIF–ALG for 24 hours (A), the diameter of the *E. coli* inhibition zone was determined, and the inhibition number (C) and the corresponding inhibition rate (D) are shown. After treatment with ZIF–NIF–ALG for 24 hours (B), the diameter of the *S. aureus* inhibition zone was determined, and the inhibition number (E) and the corresponding inhibition rate (F) are shown. *E. coli* before treatment (G) and 24 hours after treatment (H). Detection of cell contents spilled at 260 nm (I).

this indicates that the release of NIF depends on the rate of crystal disintegration.

The above experiments prove that the composite has the ability to sterilize and potentially resist inflammation; considering the potential use of the material as a therapeutic delivery platform, we then used phagocytic cells (RAW 264.7) to verify its corresponding cytocompatibility. Phagocytic cells are a commonly used bacterial infection inflammatory cell model to assess the toxicity of materials to mammalian cells. The test samples were ZIF-8, ZIF–NIF, and ZIF–NIF–ALG at concentrations ranging from 0 μg mL^{-1} to 500 μg mL^{-1}, and the cell viability was assessed after 24 h and 48 h incubation. It can be seen (Fig. 7) that the hydrogel exhibits very low cytotoxicity to

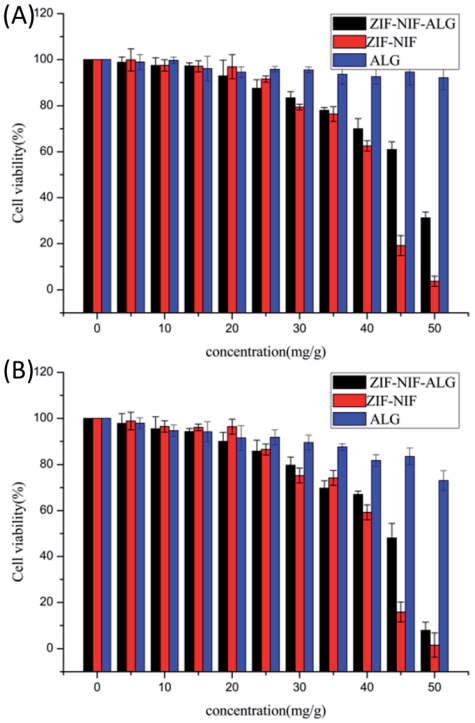

Fig. 7 (A) 24 h cell inhibition rates of ZIF–NIF\ALG\ZIF–NIF–ALG; (B) 48 h cell inhibition rates of ZIF–NIF\ALG\ZIF–NIF–ALG.

cells, ZIF–NIF–ALG exhibits significant toxicity at high doses of 200 μg mL^{-1} and 500 μg mL^{-1}, and the same weight of ZIF-8 is highly cytotoxic. This may be because ZIF–NIF–ALG carries a larger dose of Zn(II), which begins to show greater cytotoxicity at a dose of 100 μg mL^{-1}. Macrophages were exposed to this material in a dose-dependent manner, with toxicity increasing after 48 h of exposure compared to the highest dose at 24 h. When the material concentration is below 200 μg mL^{-1}, more than 90% of the phagocytic cells remain viable. The biomaterial has low cytotoxicity and addresses the problems caused by the application of the MOF material to the organism. Because the material is an *in vitro* preparation, there is no need to worry about the accumulated toxicity caused by the decomposed ligand remaining in the body. It can be applied to organisms that are infected and ulcerated, and the material can come into contact with the tissue. Metal complexes may cause hemolysis.[44] To further verify the safety of the material, we used hemolysis experiments to explore the *in vitro* biocompatibility of the material. The blood compatibility of the biological material was determined. The reaction of red blood cells with biological materials or their solution may result in the release of intracellular hemoglobin. The principle of this experiment is to measure the absorbance of the supernatant at 576 nm using a microplate reader, and the hemolytic activity can be determined as a function of hemoglobin release.[45] In this experiment, we used mouse red blood cells to detect the hemolysis caused by the biological material; the cells were incubated at 37 °C to detect the changes in the concentration of the supernatant, and it was found that the change was small. The supernatant was then examined for changes at 3 h, 6 h, 9 h, 12 h, 15 h, 18 h, 21 h, and 24 h. Finally, the biomaterial caused a hemolysis rate of 11.2% (Fig. S9†). Compared with ZIF-8 powder, the biomaterial has higher blood compatibility. This further validates that the composite hydrogel is more suitable for the human body and also lays a foundation for subsequent *in vivo* experiments.

Conclusions

In summary, ZIF–NIF–ALG is introduced as an antibacterial wound dressing. Compared with ZIF-8 and ALG, NIF and Zn(II) show a synergistic antibacterial effect, the dressing showed extraordinary bactericidal activity against *Escherichia coli* and *Staphylococcus aureus*, overcoming the defects of solid powder of the MOF. ZIF–NIF–ALG is an excellent biomaterial with pH responsiveness and sustained release. The material exhibits its antibacterial and anti-inflammatory effects by releasing metal ions and NIF, and it also shows high biocompatibility in MTT and hemolysis experiments. Therefore, ZIF–NIF–ALG has potential to be a topical antibacterial agent, and it provides promising recommendations for green, safe antibacterial agents.

Conflicts of interest

There are no conflicts to declare.

Acknowledgements

This work was supported by the Fund of National Natural Science Foundation of China (21401151), Science and Technology Support Program of Sichuan Province (2015GZ0233), Science and Technology Huimin Program of Chengdu (2015HM0100336SF), and Innovative & Practice Project of Graduate School of Southwest Jiaotong University (2018CYPY07).

References

1 X. Fan, F. Yang, J.-B. Huang, *et al.*, *Nano Lett.*, 2019, **19**, 5885–5896.
2 J. Shen, Q.-W. Wang, J. Fang, W.-X. Shen, D. Wu, G.-P. Tang and J. Yang, *RSC Adv.*, 2019, **9**, 37232–37240.
3 C.-B. He, D.-M. Liu and W.-B. Lin, *Chem. Rev.*, 2015, **115**, 11079–11108.
4 A. H. Assen, O. Yassine and O. Shekhah, *ACS Sens.*, 2017, **2**, 1294–1301.
5 X.-W. Zhang, B.-Y. Xiong, J.-J. Li, L.-B. Qian, L. Liu, Z. Liu and P. Fang, *ACS Appl. Mater. Interfaces*, 2019, **11**, 31441–31451.
6 X.-W. Zhang, B.-Y. Xiong, J.-J. Li and L.-B. Qian, *ACS Appl. Mater. Interfaces*, 2019, **11**, 31441–31451.
7 V. Andre, A. R. F. da Silva, A. Fernandes, R. Frade, C. Garcia, P. Rijo, A. M. M. Antunes, J. Rocha and M. T. Duarte, *ACS Appl. Bio Mater.*, 2019, **2**, 2347–2354.

8 R. Ballesteros-Garrido, R. Montagud-Martínez and G. Rodrigo, *ACS Appl. Mater. Interfaces*, 2019, **11**, 19878–19883.
9 H.-C. Kim, S. Mitra, M. Veerana, J.-S. Lim, H.-R. Jeong, G. Park, S. Huh, S.-J. Kim and Y. Kim, *Sci. Rep.*, 2019, **9**, 14983.
10 S. Lin, X.-M. Liu, L. Tan, Z.-D. Cui and X.-J. Yang, *ACS Appl. Mater. Interfaces*, 2017, **9**, 19248.
11 P. Li, J. Li, X. Feng, *et al.*, *Nat. Commun.*, 2019, **10**, DOI: 10.1038/s41467-019-10218-9.
12 A. Tiwari, A. Singh, N. Garg and J. K. Randhawa, *Sci. Rep.*, 2017, **7**, 12598.
13 J. Wang, Y.-M. Wang, Y.-T. Zhang, A. Uliana, J.-Y. Zhu, J.-D. Liu and B. Van der Bruggen, *ACS Appl. Mater. Interfaces*, 2016, **8**, 25508–25519.
14 X. Li, M.-L. Qi, C.-Y. Li and B. Dong, *J. Mater. Chem. B*, 2019, **7**, 6955–6971.
15 A. Malik, M. Nath, S. Mohiyuddin and G. Packirisamy, *Omega*, 2018, **3**, 8288–8308.
16 N. Bhardwaj, S. K. Bhardwaj, J. Mehta, K.-H. Kim and A. Deep, *ACS Appl. Mater. Interfaces*, 2017, **9**, 33589–33598.
17 P. Küsgens, S. Siegle and S. Kaskel, *Adv. Eng. Mater.*, 2009, **11**, 93–95.
18 W.-B. Li, Y.-F. Zhang, Q.-B. Li and G.-l. Zhang, *Chem. Eng. Sci.*, 2015, **135**, 232–257.
19 M. S. Denny, J. M. Kalaj and K. C. Bentz, *Chem. Sci.*, 2018, **9**, 8842–8849.
20 M. Liu, L. Wang, X.-H. Zheng and Z.-G. Xie, *ACS Appl. Mater. Interfaces*, 2017, **9**, 41512–41520.
21 J. Ma, S. Li, *et al.*, *J. Colloid Interface Sci.*, 2019, **553**, 834.
22 G. Wu, J.-P. Ma, *et al.*, *J. Colloid Interface Sci.*, 2018, **528**, 360.
23 J. Quiros, K. Boltes, *et al.*, *J. Colloid Interface Sci.*, 2015, **262**, 189.
24 W.-Y. Chen, H.-Y. Chang, J.-K. Lu, Y.-C. Huang, S. G. Harroun, Y.-T. Tseng, Y.-J. Li, C.-C. Huang and H.-t. Chang, *Adv. Funct. Mater.*, 2015, **25**, 7189–7199.
25 P. Rao and E. E. Knaus, *J. Pharm. Pharm. Sci.*, 2007, **11**, 81.
26 D. Kovala-Demertzi, M. Staninska, I. Garcia-Santos, A. Castineiras and M. A. Demertzis, *J. Inorg. Biochem.*, 2011, **105**, 1187–1195.
27 H. Chen, Y.-Y. Jin, J.-J. Wang, Y.-Q. Wang, W.-Y. Jiang, H. D. Dai, S.-Y. Pang, L. Lei, J. Ji and B.-L. Wan, *Nanoscale*, 2018, **10**, 20946–20962.
28 Y. Qin, L.-L. Chen, W. Pu, P. Liu, S.-X. Liu, Y. Li, X.-L. Liu, Z.-X. Lu, L.-Y. Zheng and Q.-E. Cao, *Chem. Commun.*, 2019, **55**, 2206.
29 J. Liu, J. He, L. Wang, *et al.*, *Sci. Rep.*, 2016, **6**, 23667.
30 X.-Y. Ren, C.-Y. Yang, L. Zhang, S.-H. Li, S. Shi, R. Wang, X. Zhang, T.-L. Yue, J. Sun and J.-L. Wang, *Nanoscale*, 2019, **11**, 11830.
31 X. Zhang, L.-Z. Liu, L.-J. Huang, W.-T. Zhang, R. Wang, T.-L. Yue, J. Sun, G.-L. Li and J.-L. Wang, *Nanoscale*, 2019, **11**, 9468.
32 H.-Y. Yang, L. Jiang, W. Wang and Z. F. Luo, *RSC Adv.*, 2019, **9**, 37594–37597.
33 J. Yu, W.-P. Xiong and X. Li, *Microporous Mesoporous Mater.*, 2019, **290**, 109642.
34 U. P. N. Tran, K.-K.-A. Le and N.-T.-S. Phan, *ACS. Catal.*, 2011, **2**, 120–127.
35 R. Smolkova, V. Zelenak, L. Smolko, J. Kuchar, M. Rabajdov, M. Ferencakov and M. Marekov, *Eur. J. Med. Chem.*, 2018, **153**, 131–139.
36 X. Zhang, L.-Z. Liu, L.-J. Huang, W.-T. Zhang, R. Wang, T.-L. Yue, J. Sun, G.-L. Li and J.-L. Wang, *Nanoscale*, 2019, **11**, 9468.
37 S. Mittapalli, M. K. Chaitanya Mannava, R. Sahoo and A. Nangia, *Cryst. Growth Des.*, 2019, **19**, 219–230.
38 A. Tiwari, A. Singh, N. Garg and J. K. Randhawa, *Sci. Rep.*, 2017, **7**, 12598.
39 H.-S. Rodriguez, J.-P. Hinestroza, *et al.*, *J. Appl. Polym. Sci.*, 2014, **131**, 40815.
40 L. R. Colinas, M. D. Rojas-Andrade, I. Chakraborty and S. R. J. Oliver, *CrystEngComm*, 2018, **20**, 3353–3362.
41 J. Li, X.-M. Liu, L. Tan, Z.-D. Cui, X.-J. Yang, Y.-Q. Liang, Z.-Y. Li, S.-L. Zhu, Y.-F. Zheng, K. W. Kwok Yeung, X.-B. Wang and S.-L. Wu, *Nat. Commun.*, 2019, **10**, 4490.
42 M.-F. Chung, W.-T. Chia, W.-L. Wan, Y.-J. Lin and H.-W. Sung, *J. Am. Chem. Soc.*, 2015, **39**, 12462–12465.
43 J. Ouyang, M. Wen and W.-S. Chen, *Chem. Commun.*, 2019, **55**, 4877–4880.
44 W.-X. Zhu, M. Chen, *et al.*, *Nanoscale*, 2019, **11**, 20630–20637.
45 Y. Yuan, H. Wu, H.-F. Lu, Y. Zheng, J. Y. Ying and Y.-G. Zhang, *Chem. Commun.*, 2019, **55**, 699–702.
46 G.-H. Huang, J. Chen, *et al.*, *ACS Appl. Mater. Interfaces*, 2019, **11**, 10389–10398.
47 R.-K. Alavijeh, S. Beheshti, *et al.*, *Polyhedron*, 2018, **156**, 257–278.
48 C. Tamames-Tabar, E. Imbuluzqueta, *et al.*, *CrystEngComm*, 2015, **17**, 456–462.
49 G. A. Martínez-Castañón, N. Niño-Martínez, F. Martínez-Gutierrez, *et al.*, *J.Nanopart. Res.*, 2008, **10**, 1343–1348.
50 D. F. Sava Gallis, K. S. Butler, *et al.*, *ACS Appl. Mater. Interfaces*, 2019, **11**, 7782–7791.
51 H.-S. Rodriguez, J.-P. Hinestroza, *et al.*, *J. Appl. Polym. Sci.*, 2014, **131**, 40815.